Chromium Stable Isotope Panorama of Chondrites and Implications for Earth Early Accretion

Ke Zhu, Frédéric Moynier, Conel M. O'D. Alexander, Jemma Davidson, Devin L. Schrader, Jian-Ming Zhu, Guang-Liang Wu, Martin Schiller, Martin Bizzarro, Harry Becker

The Astrophysical Journal, 923:94 (14pp), 2021 December 10 https://doi.org/10.3847/1538-4357/ac2570

Chromium Stable Isotope Panorama of Chondrites and Implications for Earth Early Accretion

Ke Zhu (朱柯)[1,2], Frédéric Moynier[1], Conel M. O'D. Alexander[3], Jemma Davidson[4], Devin L. Schrader[4], Jian-Ming Zhu[5], Guang-Liang Wu[5], Martin Schiller[6], Martin Bizzarro[6], and Harry Becker[2]
[1] Université de Paris, Institut de Physique du Globe de Paris, CNRS UMR 7154, 1 rue Jussieu, Paris F-75005, France; zhuke618@foxmail.com
[2] Freie Universität Berlin, Institut für Geologische Wissenschaften, Malteserstr. 74-100, D-12249 Berlin, Germany
[3] Earth and Planetary Laboratory, Carnegie Institution for Science, 5241 Broad Branch Road, Washington, DC 20015, USA
[4] Center for Meteorite Studies, School of Earth and Space Exploration, Arizona State University, 781 East Terrace Road, Tempe, AZ 85287-6004, USA
[5] State Key Laboratory of Geological Processes and Mineral Resources, China University of Geosciences (Beijing), Beijing 100083, People's Republic of China
[6] Centre for Star and Planet Formation, Globe Institute, University of Copenhagen, Øster Voldgade 5–7, Copenhagen DK-1350, Denmark
Received 2021 July 9; revised 2021 August 27; accepted 2021 September 8; published 2021 December 14

Abstract

We investigated the stable isotope fractionation of chromium (Cr) for a panorama of chondrites, including EH and EL enstatite chondrites and their chondrules and different phases (by acid leaching). We observed that chondrites have heterogeneous δ^{53}Cr values (per mil deviation of the $^{53}Cr/^{52}Cr$ from the NIST SRM 979 standard), which we suggest reflect different physical conditions in the different chondrite accretion regions. Chondrules from a primitive EH3 chondrite (SAH 97096) possess isotopically heavier Cr relative to their host bulk chondrite, which may be caused by Cr evaporation in a reduced chondrule-forming region of the protoplanetary disk. Enstatite chondrites show a range of bulk δ^{53}Cr values that likely result from variable mixing of isotopically different sulfide-silicate-metal phases. The bulk silicate Earth ($\delta^{53}Cr = -0.12 \pm 0.02‰$, 2SE) has a lighter Cr stable isotope composition compared to the average δ^{53}Cr value of enstatite chondrites ($-0.05 \pm 0.02‰$, 2SE, when two samples out of 19 are excluded). If the bulk Earth originally had a Cr isotopic composition that was similar to the average enstatite chondrites, this Cr isotope difference may be caused by evaporation under equilibrium conditions from magma oceans on Earth or its planetesimal building blocks, as previously suggested to explain the magnesium and silicon isotope differences between Earth and enstatite chondrites. Alternatively, chemical differences between Earth and enstatite chondrite can result from thermal processes in the solar nebula and the enstatite chondrite-Earth, which would also have changed the Cr isotopic composition of Earth and enstatite chondrite parent body precursors.

Unified Astronomy Thesaurus concepts: Chondrites (228); Isotope shifts (2069); Cosmochemistry (331); Meteorites (1038); Chemical abundances (224); Chondrules (229); Asteroids (72); Solar system (1528)

1. Introduction

Solar system planetary bodies are generally volatile depleted compared to chondritic meteorites (e.g., O'Neill & Palme 2008; Braukmüller et al. 2019). For example, Rb–Sr and K–U are elemental pairs with similar geochemical behaviors, but Rb and K are much more volatile than Sr and U, and Earth has Rb/Sr and K/U ratios that are ~10 times lower than that of Ivuna-like carbonaceous (CI) chondrites (Allègre et al. 2001; Halliday & Porcelli 2001). However, the mechanisms and conditions that led to this relative volatile-element depletion remain ambiguous. The stable isotopes of elements can be fractionated by volatilization processes and the shifts in their isotopic compositions have been applied to understand volatile-element depletion processes (Humayun & Clayton 1995; Luck et al. 2005; Hin et al. 2017; Kato & Moynier 2017b; Pringle & Moynier 2017; Young et al. 2019; Bloom et al. 2020; Hellmann et al. 2021). Cr is a moderately volatile element (Lodders 2003; Wood et al. 2019) that may show a special behavior during volatilization at higher temperatures. Under moderately reducing to oxidizing conditions ($fO_2 > IW+1$), relevant during evaporation processes from magma oceans on planets (Visscher & Fegley 2013), Cr may be present in the gas as oxide species CrO(g), CrO_2(g) and CrO_3(g) (Chase 1998). Equilibrium isotopic fractionation between these gas phase species and melt will cause enrichment of the lighter Cr isotopes in the condensed phases, in which Cr is either di- or trivalent, relative to the vapor (Sossi et al. 2018). This contrasts with its speciation under more reduced nebular conditions in which Cr may be present as Cr^{2+} (major; in silicates) or Cr^0 (minor; in Fe–Ni metal) in condensed phases and Cr^0 in the gas (Grossman et al. 2008), in which case, through either equilibrium or kinetic fractionation, the condensed phase will be enriched in the heavy Cr isotopes. Solids or magmas that evaporated significant quantities of moderately volatile elements such as Zn, K, Rb, or Ga normally show enrichments of heavy isotopes of these elements, both for kinetic and equilibrium isotope fractionation processes (Paniello et al. 2012; Wang & Jacobsen 2016; Kato & Moynier 2017a; Pringle & Moynier 2017). The behavior of Cr during evaporation has been a motivation to apply this element to study the origin of volatile depletion in the Moon and of the eucrite parent body (likely asteroid 4-Vesta) (Sossi et al. 2018; Zhu et al. 2019b). Both lunar samples and HED meteorites from Vesta are enriched in the lighter isotopes of Cr compared to Earth and chondrites. These isotopic enrichments have been interpreted to reflect equilibrium Cr isotope fractionation between melt (reduced, and enriched in CrO) and gas (oxidized, and enriched in CrO_2) during evaporation from a magma ocean. Given that at equilibrium, isotopic fractionation scales with $1/T^2$, the Cr evaporation from the Moon and Vesta was estimated to have occurred under relatively low temperatures (~2000 K), which in the case of the Moon is comparable to the surface temperature of a lunar magma ocean (Sossi et al. 2018).

Some chondrites host the oldest dated known materials of the early solar system, the most pristine of which preserve information about the origin of the solar system (e.g., Krot et al. 2014). As opposed to planets and differentiated asteroids, chondrite parent bodies did not undergo significant melting (though most underwent varying degrees of thermal metamorphism and aqueous alteration) and thus did not differentiate into a core and mantle. Hand specimens of bulk chondrites have chemical compositions that, for some elements (e.g., Cr), are often taken as representative of their bulk parent bodies and are sometimes used as proxies for the composition of the building materials of terrestrial planets such as Earth (Allègre et al. 1995; Javoy et al. 2010; Palme & O'Neill 2014). Because the building materials of Earth may have undergone volatility-controlled fractionation processes in the nebula or by magma ocean degassing, Cr stable isotope compositions of chondrites may help to unravel the details of these processes.

Previous studies have precisely estimated the Cr stable isotope composition of the bulk silicate Earth (expressed as the δ^{53}Cr value; per mil deviation of the $^{53}Cr/^{52}Cr$ ratio from the NIST SRM 979) to be –0.12 ± 0.04‰ (2SD; Schoenberg et al. 2008; Sossi et al. 2018; Jerram et al. 2020), which is indistinguishable from the presently estimated average chondritic value, –0.12 ± 0.04‰ (2SD, $N = 42$; Bonnand et al. 2016; Schoenberg et al. 2016; Zhu et al. 2021b). However, among the different groups of chondrites, the Cr stable isotope compositions of the enstatite chondrites (ECs) are not well established as they are based on only two samples, Indarch (EH4) and Khairpur (EL6) with two distinct values: –0.10 ± 0.01 and –0.05 ± 0.01, respectively (Bonnand et al. 2016). This is somewhat problematic as the ECs (including their chondrules) usually provide the best match to the isotopic composition of the bulk silicate Earth for most elements (Javoy et al. 2010; Moynier & Fegley 2015), and particularly for Earth's non-mass-dependent Cr isotopic composition (Trinquier et al. 2007; Qin et al. 2010; Mougel et al. 2018; Zhu et al. 2020b). On the other hand, chondrules, the major components in chondrites (Hewins 1997), are volatile depleted (Scott & Krot 2014; Pringle et al. 2017; Mahan et al. 2018). Chondrules are some of the oldest solar system solids (Connelly et al. 2012; Schrader et al. 2017; Zhu et al. 2019a, 2020b), but their precise formation mechanisms are still unclear. Some authors also proposed that the terrestrial planets may have formed predominantly from chondrules (Johansen et al. 2015, 2021; Yoshizaki & McDonough 2021). Therefore, evaluating the Cr stable isotope compositions of the ECs and their chondrules may help unravel the formation history of Earth and EC parent bodies.

The apparent Cr stable isotope homogeneity suggested by previous studies of bulk chondrites (Bonnand et al. 2016; Schoenberg et al. 2016; Zhu et al. 2021b) is surprising, given the heterogeneous mass-dependent isotopic compositions of other elements, e.g., Si (Armytage et al. 2011), Fe (Wang et al. 2014), Ni (Klaver et al. 2020; Wang et al. 2021), Ca (Schiller et al. 2015, 2018; Huang & Jacobsen 2017), or Zn (Luck et al. 2005; Pringle et al. 2017). However, the Cr stable isotope composition of most ungrouped chondrites, as well as of several distinct chondrite groups, such as CB, CH, CK, CR, and Kakangari chondrite (KC) are still unknown. As such, expanding the overall Cr stable isotope data set will make it possible to further evaluate potential mass-dependent Cr isotope variability between chondrites and may provide insights into the evolution conditions of the nebula and chondrite parent body processes. Given the approach of using chondrites as representative materials for the precursor materials of the terrestrial planets, further understanding the Cr stable isotope compositions of chondrites is essential to form a baseline for using Cr isotopes as tracers of the volatile-element history of differentiated planetary bodies.

Here, we employ both multiple-collector inductively coupled-plasma mass-spectrometry (MC-ICP-MS) and thermal-ionization mass-spectrometry (TIMS) combined with a double spike (DS) method to report the high-precision Cr stable isotope compositions for a series of chondrites, including bulk EH and EL groups of ECs, eight groups (CI, CB, CH, CR, CM, CO, CV, and CK) of carbonaceous chondrites (CCs), H ordinary chondrites (OCs), one KC, and 17 ungrouped CC and non-CC chondrites. On the basis of these data, we provide new constraints on the volatilization processes that affected Cr in presumed Earth's precursor bodies and the origins of the chondrite parent bodies. In addition, we also report the Cr stable isotope data for three chondrules extracted from one of the most primitive EH3 chondrite (SAH 97096). Lastly, we investigate the Cr isotope heterogeneity between EC components, based on the Cr stable isotope compositions of leachates of different fractions (magnetic, nonmagnetic sulfide-rich, and nonmagnetic silicate-rich) that were separated magnetically and chemically from three ECs of varying metamorphism grades.

2. Samples and Analytical Methods

Most Cr stable isotope data for bulk meteoritic samples were from using the same dissolutions previously utilized in Zhu et al. (2021c), Pedersen et al. (2019), and Zhu et al. (2020b) that reported mass-independent Cr isotopic compositions. Note that, Pedersen et al. (2019) has already reported the mass-dependent Cr isotope data of the OCs measured using the sample-standard bracketing (SSB) method. Here, we employed DS techniques, and compare the data measured by the two methods in Appendix A.1 Table A1 and Figure A1. The individual chondrules were extracted as part of the study by Zhu et al. (2020b) that reported mass-independent Cr isotope data for individual chondrules. Their backscattered electron (BSE) images are reported in Appendix A.2 and Figure A2. In addition to these data, we further selected nine EL and 10 EH chondrites covering the petrological types of EL3–6 and EH3–5, one KC sample (LEW 87232, K3), and 17 ungrouped chondrites, including 14 carbonaceous (CCs) and three non-carbonaceous chondrites (non-CCs), for which mass-independent Cr isotope compositions have been previously reported in Zhu et al. (2021a). Sample information is listed in Table 1.

The ECs (except for SAH 97096) and ungrouped chondrites were first ground into powders from ∼1 g and 0.1–1 g meteorite pieces, respectively, and 5–100 mg aliquots of the powders were weighed for Cr analyses (Table 1). Note that Stracke et al. (2012) argued that ∼0.6 g of chondrite (Allende, CV) is enough to be representative of bulk chondrite composition. Since all the EC samples in this study were ∼1 g, the aliquots of the homogenized powders analyzed here should be representative of the bulk meteorite compositions. All the samples were dissolved in Teflon bombs + Evapo Clean (Inglis et al. 2018; Zhu et al. 2021b) at 140°C using concentrated HF + HNO_3 (2:1) for ∼2 days and concentrated aqua regia (HCl + HNO_3, 3:1) at 140°C for another 2 days following a protocol described in Inglis et al. (2018), and previously used for Cr isotopic measurements (Zhu et al. 2020a, 2020b, 2021b, 2021c). Detailed sample information can be found in Table 1. To assess the accuracy and reproducibility

Table 1
Cr Stable Isotope Compositions of Chondrites and Reference Standards

Sample Name	Type	Mass (mg)	δ^{53}Cr	2SD	N/References	Instruments
CCs						
Orgueil	CI1	22.6	−0.15	0.02	4	MC-ICP-MS
Orgueil	CI1	…	−0.15	0.01	1/[1]	TIMS
Average			−0.15	0.01	2SD	
Alais	CI1	…	−0.16	0.04	[2]	MC-ICP-MS
MIL 05082 (chunk)	CB3	96.4	−0.20	0.02	2	MC-ICP-MS
QC 001	CBa3	39.8	−0.18	0.04	3	MC-ICP-MS
PCA 91467	CH3	28.5	−0.12	0.03	3	MC-ICP-MS
A-881020	CH3	40.5	−0.19	0.04	3	MC-ICP-MS
GRO 95577	CR1	20.5	−0.14	0.03	2	MC-ICP-MS
Al Rais	CR2-an	23.2	−0.16	0.02	2	MC-ICP-MS
SCO 06043	CM1	21.7	−0.11	0.02	3	MC-ICP-MS
Nogoya	CM2	24.3	−0.08	0.03	2	MC-ICP-MS
Banten	CM2	21.7	−0.09	0.02	2	MC-ICP-MS
Murchison	CM2	…	−0.12	0.01	1/[1]	TIMS
Mighei	CM2	…	−0.11	0.04	[2]	MC-ICP-MS
MIL 07193	CO3	20.9	−0.09	0.02	2	MC-ICP-MS
DOM 10104	CO3	24.7	−0.10	0.04	2	MC-ICP-MS
Ornans (chunk)	CO3	66.2	−0.07	0.01	1/[1]	TIMS
Axtell	CV3	…	−0.14	0.04	[2]	MC-ICP-MS
SaU 040	CV3	…	−0.09	0.04	[2]	MC-ICP-MS
Allende	CV3-oxA	∼100	−0.13	0.02	2	MC-ICP-MS
Allende	CV3-oxA	…	−0.11	0.01	1/[1]	TIMS
Allende	CV3-oxA	…	−0.12	0.04	[2]	MC-ICP-MS
Average		…	−0.12	0.02	2SD	…
Bali	CV3-oxB	42.3	−0.12	0.02	2	MC-ICP-MS
Mokoia	CV3-oxB	20.5	−0.13	0.02	2	MC-ICP-MS
Leoville	CV3-red	24.8	−0.11	0.02	2	MC-ICP-MS
Vigarano	CV3-red	21.0	−0.13	0.02	2	MC-ICP-MS
Kaba	CV3-oxB	19.7	−0.12	0.02	2	MC-ICP-MS
Kaba	CV3-oxB	…	−0.13	0.04	[2]	MC-ICP-MS
Average			−0.13	0.02	2SD	
ALH 85002	CK4	45.8	−0.13	0.02	3	MC-ICP-MS
Karoonda	CK4	33.9	−0.13	0.02	2	MC-ICP-MS
EET 92002	CK5	34.6	−0.14	0.05	2	MC-ICP-MS
LEW 87009	CK6	43.8	−0.14	0.02	2	MC-ICP-MS
OCs						
Roosevelt	H3.4	63–260	−0.10	0.02	2	MC-ICP-MS
Brownsflied	H3.7	63–260	−0.08	0.04	3	MC-ICP-MS
Ochansk	H4	63–260	−0.09	0.02	2	MC-ICP-MS
Beaver Creek	H4	63–260	−0.08	0.02	2	MC-ICP-MS
Bath	H4	63–260	−0.09	0.02	2	MC-ICP-MS
Menow	H4	63–260	−0.10	0.02	2	MC-ICP-MS
Djoumine	H5-6	…	−0.11	0.04	[2]	MC-ICP-MS
Forest city	H5	63–260	−0.11	0.04	3	MC-ICP-MS
Aarhus	H6	63–260	−0.11	0.02	2	MC-ICP-MS
Estacado	H6	63–260	−0.09	0.02	2	MC-ICP-MS
Portales Valley	H6/7	63–260	−0.04	0.06	2	MC-ICP-MS
Dubrovnik	L3-6	…	−0.10	0.04	[2]	MC-ICP-MS
Barratta	L4	…	−0.12	0.01	1/[1]	TIMS
Homestead	L5	…	−0.10	0.04	[2]	MC-ICP-MS
Bruderheim	L6	…	−0.11	0.01	1/[1]	TIMS
Parnallee	LL3	…	−0.12	0.01	1/[1]	TIMS
Soko-Banja	LL4	…	−0.12	0.04	[2]	MC-ICP-MS
Dar al Gani 298	LL4	…	−0.10	0.04	[2]	MC-ICP-MS
ECs						
MAC 88184	EL3	4.6	−0.03	0.04	3	MC-ICP-MS
MAC 02837	EL3	6.5	−0.02	0.03	3	MC-ICP-MS
MAC 02747	EL4	5.5	0.01	0.03	3	MC-ICP-MS
Eagle	EL6	7.1	0.01	0.02	3	MC-ICP-MS
Khairpur	EL6	5.5	0.00	0.04	3	MC-ICP-MS
Khairpur	EL6	…	−0.05	0.01	1/[1]	TIMS
Average			−0.02	0.07	2SD	
LON 94100	EL6	5.8	−0.09	0.04	3	MC-ICP-MS
Pillistfer	EL6	6.3	0.09	0.02	2	MC-ICP-MS
Hvittis	EL6	7.9	−0.13	0.05	5	MC-ICP-MS
Atlanta	EL6	6.6	−0.12	0.04	3	MC-ICP-MS
Kota-Kota	EH3	7.5	−0.03	0.02	3	MC-ICP-MS
GRO 95517	EH3	7.8	−0.05	0.02	3	MC-ICP-MS

Table 1
(Continued)

Sample Name	Type	Mass (mg)	δ^{53}Cr	2SD	N/References	Instruments
CCs						
QingZhen	EH3	5.5	−0.06	0.02	5	MC-ICP-MS
MIL 07028	EH3	7.2	−0.29	0.03	3	MC-ICP-MS
SAH 97096 (powder)	EH3	33.2	−0.07	0.02	2	MC-ICP-MS
SAH 97096 (chunk)	EH3	∼100	−0.13	0.02	2	TIMS
Average			−0.10	0.09	2SD	
Abee	EH4	8.5	−0.04	0.02	3	MC-ICP-MS
Indarch	EH4	11.8	−0.11	0.02	3	MC-ICP-MS
Indarch	EH4	…	−0.10	0.01	1/[1]	TIMS
Average		…	−0.11	0.01	2SD	
EET 96135	EH4/5	8.8	−0.04	0.04	5	MC-ICP-MS
EET 96299	EH4/5	8.7	−0.04	0.04	5	MC-ICP-MS
St. Mark's	EH5	6.3	−0.05	0.02	4	MC-ICP-MS
RCs						
Average	R3-6		−0.12	0.04	[3]	MC-ICP-MS
KC						
LEW 87232 (chunk)	K3	45.7	0.32	0.02	2	MC-ICP-MS
LEW 87232 (repeat)	K3	…	0.29	0.02	2	TIMS
Average			0.30	0.03		
Ungrouped chondrites						
Tagish Lake	C2-ung	19.8	−0.13	0.02	2	MC-ICP-MS
Bells	C2-ung	20.1	−0.19	0.02	2	TIMS
QUE 99038	C2-ung	20.8	−0.16	0.02	2	MC-ICP-MS
MAC 87300	C2-ung	107.5	−0.12	0.02	2	TIMS
MAC 87301	C3-ung	57.7	−0.09	0.02	2	TIMS
MAC 88107	C3-ung	50.0	−0.10	0.02	2	TIMS
DaG 430	C3-ung	23.9	−0.21	0.02	2	TIMS
DaG 429	C3-ung	39.3	−0.15	0.02	2	TIMS
NWA 1152	C3-ung	26.1	−0.13	0.02	2	TIMS
NWA 12416	C3-ung	20.9	−0.14	0.02	2	TIMS
DaG 978	C3-ung	21.6	−0.15	0.02	2	TIMS
MIL 090001	CR2/C2-ung	37.0	−0.11	0.02	2	TIMS
BUC 10933 (powder 1)	CR2/C2-ung	33.2	−0.13	0.02	2	TIMS
BUC 10933 (powder 2)	CR2/C2-ung	22.5	−0.15	0.02	2	MC-ICP-MS
Average			−0.14	0.03		
MIL 07513 (powder 1)	CR2/C2-ung	33.4	−0.17	0.02	2	TIMS
MIL 07513 (powder 2)	CR2/C2-ung	20.9	−0.13	0.02	2	MC-ICP-MS
Average			−0.15	0.06		
MIL 15362	Chondrite-ung	48.7	−0.07	0.03	2	TIMS
GRO 95551	Chondrite-ung	72.4	−0.15	0.02	2	TIMS
NWA 5717	Chondrite-ung	45.4	−0.10	0.02	2	TIMS
Reference Standards						
NIST 3112a	Pure Cr		−0.07	0.02	8	MC-ICP-MS
NIST 3112a	Pure Cr		−0.05	0.02	9	TIMS
NIST 3112a	Pure Cr		−0.08	0.03	5/[6]	MC-ICP-MS
NIST 3112a	Pure Cr		−0.04	0.02	25	MC-ICP-MS
Average			−0.06	0.04	2SD	
DTS-1	Dunite	∼100	−0.09	0.04	9	MC-ICP-MS
DTS-1	Dunite		−0.12	0.03	3	MC-ICP-MS
DTS-1	Dunite		−0.07	0.05	4	MC-ICP-MS
DTS-1	Dunite		−0.08	0.02	2	TIMS
DTS-1	Dunite		−0.08	0.04	2/[4]	MC-ICP-MS
DTS-1	Dunite		−0.03	0.03	5/[6]	MC-ICP-MS
Average			−0.08	0.06	2SD	
PCC-1	Peridotite	∼100	−0.10	0.03	4	MC-ICP-MS
PCC-1	Peridotite		−0.09	0.05	3	MC-ICP-MS
PCC-1	Peridotite		−0.09	0.02	2	MC-ICP-MS
PCC-1	Peridotite		−0.04	0.03	3	TIMS
PCC-1	Peridotite		−0.10	0.04	2/[4]	MC-ICP-MS
PCC-1	Peridotite		−0.08	0.05	3/[3]	MC-ICP-MS
PCC-1	Peridotite		−0.04	0.03	6/[6]	MC-ICP-MS
Average			−0.08	0.06	2SD	
BHVO-2	Basalt	∼100	−0.11	0.02	1	MC-ICP-MS
BHVO-2	Basalt		−0.14	0.02	3	MC-ICP-MS
BHVO-2	Basalt		−0.13	0.02	3	TIMS
BHVO-2	Basalt		−0.11	0.02	9	TIMS

Table 1
(Continued)

Sample Name CCs	Type	Mass (mg)	δ^{53}Cr	2SD	N/References	Instruments
BHVO-2	Basalt		−0.13	0.04	1/[4]	MC-ICP-MS
BHVO-2	Basalt		−0.11	0.03	2/[3]	MC-ICP-MS
BHVO-2	Basalt		−0.10	0.03	4/[5]	MC-ICP-MS
BHVO-2	Basalt		−0.15	0.03	2/[6]	MC-ICP-MS
Average			−0.12	0.03	2SD	

Note. We did not consider the following literature δ^{53}Cr data (Bonnand et al. 2016; Schoenberg et al. 2016): Kernouve, Dar al Gani 300, Bath, Cereseto, Bremervörde, Borkut, Mt Tazerzait, Dhurmsala, Saint-Severin, and Mokoia, with mass-independent Cr isotope compositions (i.e., ε^{53}Cr and ε^{54}Cr values) that are inconsistent (difference $>\sim$0.5 for ε^{54}Cr) with other studies (Trinquier et al. 2007, 2008b; Qin et al. 2010; Mougel et al. 2018; Pedersen et al. 2019; Zhu et al. 2021c).
References. (1) Bonnand et al. [2016], (2) Schoenberg et al. [2016], (3) Zhu et al. [2021b], (4) Zhu et al. [2019b], (5) Sossi et al. [2018], and (6) Zhu et al. [2021d]. Note that, the data for reference standards reported in the table are only from our labs (Institut de Physique du Globe de Paris and Freie Universität Berlin).

of the data acquired in this study, we also measured the Cr stable isotopic compositions of the well-studied meteorite Allende (CV3), the pure Cr standard NIST 3112a, and three United States Geological Survey (USGS) reference rock standards: DTS-1 (dunite), PCC-1 (peridotite), and BHVO-2 (basalt).

For the acid leaching of the three ECs, Qingzhen (EH3), Khairpur (EL6), and Indarch (EH4), we followed the same protocol used in Moynier et al. (2011a) prior to Zn isotopic measurements. In summary, the magnetic fractions (from sample powders) were collected using a hand magnet, and dissolved in aqua regia in Teflon bombs at 140°C for 2 days. Note that the magnetic fractions cannot be pure metal and must include other Fe–Ni-bearing minerals. After extraction of the magnetic fraction, the residual nonmagnetic fraction was then dissolved from the samples in cold 3N HCl for ∼6 hr to extract the sulfides. The final residues (mostly silicates) were dissolved in concentrated HF + HNO_3 at 140°C for 2 days and concentrated aqua regia at 140°C for another 2 days in Teflon bombs to dissolve the residue silicates.

Sample fractions containing 3–5 μg of Cr were taken out of the dissolved solution and were doped with a ^{50}Cr–^{54}Cr spike mixing with spike proportion ratios from 25% to 30% (Sossi et al. 2018). The sample-spike mixtures were heated at 120°C on a hotplate overnight to ensure sample-spike equilibrium, and then dried down before column chemistry. To purify Cr in all the samples, we used the two-step column chemistry first described in Trinquier et al. (2008a) and routinely applied in our previous studies (Sossi et al. 2018; Zhu et al. 2019b, 2021b) at IPGP. The Cr yield is typically ∼75%, but ranges from 60%–90% for some samples, and the total blank was ∼2 ng. The DS techniques correct for any Cr stable isotope fractionation during the chemical purification as a result of yields not being 100%.

The Cr stable isotope compositions of most of the purified CC and OC samples were measured on a Thermo Scientific Neptune Plus MC-ICP-MS housed at the IPGP. Analytical details are described in Zhu et al. (2021b, 2021d), Sossi et al. (2018) and Zhu et al. (2019b). The purified sample solution was diluted to ∼1 ppm, which typically returns a signal of ∼15 V with a nebulizer flow rate of 50 μl minute^{-1}, using the Stable Introduction System (SIS). Every measurement was composed of 100 cycles, with a baseline of 30 s and integration time of 4.194 s for each cycle, a standard was analyzed after every two or three samples.

For most of the ungrouped chondrites, we use a Thermo Finnigan Triton TIMS at Freie Universität Berlin to measure their Cr stable isotope compositions. The purified Cr cuts of the samples were dissolved in 100–200 μl 30% H_2O_2, and heated at 70°C on a hotplate for 0.5–1 hr. In this way, the Cr will be converted into Cr^{6+} (in purple). This step is important to remove organics from the resin which are detrimental for Cr ionization by TIMS. The low-temperature H_2O_2 method for removing organics appears to be much more effective than the HNO_3, aqua regia, and adverse aqua regia (i.e., HNO_3:HCl = 3:1) that was used in our previous studies, because we found that the Cr prepared in this way ionized more efficiently by TIMS, producing a higher and longer lasting signal for the same ionization temperature and sample load. Then, 0.5 ml of 6 N HCl was added to the sample and dried down to transfer the Cr into HCl media before loading the sample onto TIMS filaments. Another way to decrease the influence of organics is to dilute the samples when they are loaded onto the filaments. Only ∼500 ng of Cr was loaded on a single filament from a total of 10–20 μg of Cr. Thus, any remaining organics on the filament were diluted 20–40 times. Through monitor isotope signals of ^{49}Ti, ^{51}V, and ^{56}Fe, we correct the isobaric effects of ^{50}Ti, ^{50}V ,and ^{54}Fe on ^{50}Cr and ^{54}Cr, respectively.

The purified samples and reference materials were loaded onto degassed Re filament, mixed with 0.5 μl Al-doped Si gel and 0.5 μl concentrated boric acid, and the mixed liquid was quickly dried down within 1 minute by heating the filaments with a current of ∼1.5 A in air. Then the current was turned up to >2 A, until the color of the filament turned to dull red for ∼1 s, to form a glass, before loading it onto the TIMS turret. After ∼5 hr of pumping the turret and the HV pressure dropped to below 5 × 10^7 kPa, we started the automatic measurement sequence. A liquid N_2 cold finger was not needed to further decrease the HV pressure. Similar to measurements on MC-ICP-MS, every measurement on TIMS is composed of 100 cycles, with a ^{52}Cr beam of ∼15 V, a baseline measurement of 30 s and a sample integration time of 4.194 s for each cycle, and after every two to three samples a standard was run for bracketing of the samples. We compare the δ^{53}Cr data measured by MC-ICP-MS and TIMS in Appendix A.3 and Figure A3.

Because of the small sample sizes for the chondrule analyses, we employed the Neptune Plus MC-ICP-MS housed at China University Geoscience (Beijing) with an Aridus II + ice

chamber introduction system described in Wu et al. (2020). The three chondrules from EH3 chondrite SAH 97096 (Zhu et al. 2020b) were purified by the protocol described in Zhu et al. (2018), and their Cr isotope ratios were measured by the method described in Wu et al. (2020). Every measurement was composed of 60 cycles, with an integration time of 4.194 s for each cycle and a ^{52}Cr beam of ~15 V (50 ppb of Cr). For the baseline, the blank of 2.5% HNO_3 was measured for 120 s on peak and subtracted from subsequent sample signals.

Relative to terrestrial samples, meteorites usually possess Cr isotopic anomalies (Zhu et al. 2021c), i.e., the mass-independent Cr isotope fractionations that were expressed as ε^{53}Cr and ε^{54}Cr (ε indicates the per 10,000 isotope deviation relative to standards). Although mass-dependent Cr isotope fractionation focuses on ^{53}Cr/^{52}Cr ratios, we also need to consider the ε^{54}Cr values, since we used the ^{54}Cr spike. The effects of the Cr isotopic anomalies on the final δ^{53}Cr values for ECs and EC leachates were corrected using their average ε^{53}Cr (0.16 ± 0.06) and ε^{54}Cr (0.02 ± 0.11) values (Trinquier et al. 2007; Qin et al. 2010; Mougel et al. 2018; Zhu et al. 2021c), while those of the CCs, OCs, and ungrouped chondrites were corrected using their respective mass-independent Cr isotope compositions that had previously been analyzed on the same sample solutions (Pedersen et al. 2019; Zhu et al. 2021a, 2021c) and literature data (Petitat et al. 2011; Torrano et al. 2021). Note that, the silicate fractions of the ECs also possess ε^{54}Cr of ~0.1 (Qin et al. 2010), and ε^{53}Cr and ε^{54}Cr values of 1 ε only result in δ^{53}Cr differences of <0.01 and <0.04, respectively (Zhu et al. 2019b). Hence, using the bulk ε^{53}Cr and ε^{54}Cr values of the ECs is acceptable for representing the EC non-magmatic fractions and correcting their Cr isotope anomalies (mass-independent isotope fractionation). As for the magnetic fractions (with high Fe/Cr ratios) from EC leachates, we also report the calculated δ^{53}Cr values (relative to the measured δ^{53}Cr values) by the mass-balance calculation: bulk δ^{53}Cr value are contributed by the sum of three fractions, i.e., magnetic, nonmagnetic sulfides, and nonmagnetic silicates. Due to the small sample sizes, the entire samples were needed for the stable isotope measurements and we could not measure their mass-independent Cr isotope ratios. Thus, we could not make any corrections for Cr isotope anomalies. However, the magnitude of the ε^{53}Cr and ε^{54}Cr variation reported previously ~–0.2 to ~+0.5 and from ~–0.2 to ~+1.0 (Zhu et al. 2020b), would only cause the DS δ^{53}Cr data to be shifted by ~0.02 (Zhu et al. 2019b), which is within our data uncertainty. For the phases separated from the ECs we assumed that they all had the same ε^{53}Cr (0.16) and ε^{54}Cr (0.02) (Zhu et al. 2021c) as bulk ECs.

The Cr stable isotopic ratios for all samples in this study are reported in delta notation relative to NIST SRM 979:

$$\delta^{53}\mathrm{Cr}(‰) = \left(\frac{(^{53}\mathrm{Cr}/^{52}\mathrm{Cr})_{\mathrm{sample}}}{(^{53}\mathrm{Cr}/^{52}\mathrm{Cr})_{\mathrm{NIST\ SRM\ 979}}} - 1 \right) \times 1000. \quad (1)$$

The uncertainties quoted for individual samples are the 2SD of individual sample measurements (at least two measurements) or the 2SD reproducibility of several NIST SRM 979 measurements in the same analytical session, whichever is larger, i.e., 0.022‰ for MC-ICP-MS and 0.017‰ for TIMS, whichever is the largest. The data for NIST 3112a, BHVO-2, DTS-1, PCC-1, Orgueil, Allende, Kaba, Khairpur, and Indarch are highly consistent with previous studies (Bonnand et al. 2016; Schoenberg et al. 2016; Sossi et al. 2018; Zhu et al. 2018, 2019b; Wu et al. 2020). Note that, the meteorite data that were used for data comparisons here are consistent with ε^{53}Cr and ε^{54}Cr values, i.e., their ε^{53}Cr and ε^{54}Cr differences relative to those in the literature (Trinquier et al. 2007; Qin et al. 2010; Zhu et al. 2021c) are less than 0.5, respectively. There are also no obvious differences between results for the same samples that were measured by MC-ICP-MS and TIMS (Figure A3), except for bulk SAH 97096 (two chunks) that can be ascribed to sample heterogeneity.

3. Results

The δ^{53}Cr values for bulk chondrites, terrestrial rock standards (BHVO-2, PCC-1, and DTS-1) and NIST 3112a are reported in Table 1, whereas those for EC chondrules and leachates (including leachates of magnetic components, nonmagnetic sulfide-rich, and nonmagnetic silicate-rich fractions) are reported in Tables 2 and 3, respectively. We also include some δ^{53}Cr values from previous works (Bonnand et al. 2016; Schoenberg et al. 2016) that are corrected by consistent mass-independent Cr isotope compositions, i.e., ε^{53}Cr and ε^{54}Cr values, using well-established literature data (Trinquier et al. 2007; Qin et al. 2010; Zhu et al. 2021c).

Combining our new data with literature data shows that the bulk Cr stable isotope compositions among chondrites range from –0.29 ± 0.03‰ for MIL 07028 (EH3) to +0.30 ± 0.03‰ for LEW 87232 (K) (Figure 1). The H, L, and LL OCs have indistinguishable δ^{53}Cr values with an average of –0.10 ± 0.04‰ (2SD, $N = 28$). We also compared the δ^{53}Cr data of H chondrites obtained on different aliquots from the same sample digestions measured by DS and SSB methods (with a yield of 99%; Pedersen et al. 2019) methods (Appendix A.1). Apart from one sample (Aarhus), the data obtained by the two methods are in excellent agreement with each other given their respective analytical uncertainties (2SD = 0.05‰ for the SSB data; Schiller et al. 2014). There is resolved δ^{53}Cr variability between some CC groups, e.g., CI and CB chondrites have lighter isotopic compositions compared to the other CCs such as the CM, CO, CV, and CK chondrites. Within a group, all the CCs have indistinguishable δ^{53}Cr values, independent of the degree of aqueous alteration (e.g., petrologic types 1 and 2) they have experienced, and their oxidation states (e.g., different CV subgroups: CV_{oxA}, oxidized Allende-like; CV_{oxB}, oxidized Bali-like, and CV_{red} reduced Vigarano-like). The ungrouped chondrites record variable δ^{53}Cr values that range from –0.21 ± 0.01‰ for DaG 430 (C3-ungrouped) to –0.07 ± 0.03‰ for MIL 15362 (chondrite-ung.), and there are no systematic δ^{53}Cr differences between ungrouped CCs and non-CCs.

ECs show considerable intragroup δ^{53}Cr variability that ranges from –0.29 ± 0.03‰ for MIL 07028 (EH3) to –0.03 ± 0.02‰ for Kota-Kota (EH3), and from −0.13‰ ± 0.05‰ for Hvittis (EL6) to 0.09 ± 0.02‰ for Pillistfer (EL6). Excluding MIL 07028 and Hvittis, which have the most extreme δ^{53}Cr values, the remaining ECs have an average δ^{53}Cr composition of –0.05 ± 0.08‰ (2SD, $N = 17$) that is higher than that of most other chondrite groups. There is no resolvable δ^{53}Cr difference between the EL (–0.05 ± 0.11‰, 2SD; $N = 8$) and EH (–0.06 ± 0.05‰, 2SD; $N = 9$) groups.

The δ^{53}Cr values of acid leachates (performed via the same leaching procedure described in Moynier et al. 2011a and described in Appendix A.1) of three ECs vary from heavy Cr

Table 2
Cr Stable Isotope Compositions of Acid Leachates of Separated Fractions of ECs

Samples	Mass (mg)	Cr Concentration (ppm)	Cr Content (ug)	δ^{53}Cr	2SD	*N*
Qingzhen (EH3)						
Bulk	71.3	…	…	–0.06	0.02	5
Magnetic—measured	48.3	4251	63.0	–0.23	0.03	3
Magnetic—calculated	…	…	…	–0.02	0.05	…
Nonmagnetic sulfides	8.2	1476	12.1	–0.12	0.03	3
Nonmagnetic silicates	14.8	1358	20.1	–0.16	0.02	3
Indarch (EH4)						
Bulk	85.1	…	…	–0.11	0.02	3
Magnetic—measured	63.3	1591	100.7	–0.21	0.03	3
Magnetic—calculated	…	…	…	–0.19	0.03	…
Nonmagnetic sulfides	9.0	3656	32.9	0.27	0.03	3
Nonmagnetic silicates	12.8	2828	36.2	–0.23	0.01	3
Khairpur (EL6)						
Bulk	47.1	…	…	0.00	0.04	3
Magnetic—measured	11.8	1229	14.5	–0.05	0.04	3
Magnetic—calculated	…	…	…	0.06	0.06	…
Nonmagnetic sulfides	8.0	3775	30.2	0.92	0.02	3
Nonmagnetic silicates	27.3	4081	111.4	–0.25	0.03	3

Note. All the δ^{53}Cr values for ECs and EC fractions are corrected for their potential Cr isotopic anomalies (mass-independent Cr isotope fractionation) with average ε^{53}Cr (0.16) and ε^{54}Cr (0.02) (Trinquier et al. 2007, 2008b; Qin et al. 2010; Mougel et al. 2018; Zhu et al. 2021c). Although silicate fractions in ECs have bulk-like ε^{53}Cr and ε^{54}Cr values, while the magnetic fractions (with high Fe/Cr ratios) have elevated ε^{53}Cr and ε^{54}Cr values, mostly by cosmogenic effects (Qin et al. 2010). Hence, it is not acceptable to correct their isotope anomalies by using the bulk ε^{53}Cr and ε^{54}Cr values of ECs (δ^{53}Cr value of "Magnetic—measured"), and we calculate their more accurate δ^{53}Cr values ("Magnetic—calculated") by mass balance. The δ^{53}Cr data of bulk chondrites refer to those in Table 1 (e.g., the mass information). The precision for the Cr concentration and content measured by ICP-MS is estimated as ∼10%.

Table 3
Cr Stable Isotope Compositions of Chondrules from SAH 97096 EC

Sample	δ^{53}Cr	2SD	*N*	Mg#	Fe/Cr	Na/Al	Mn/Cr	Mg/Ni
KF3	0.05	0.03	3	93%	12.4	2.64	0.33	964
KF10	–0.04	0.04	3	75%	42.5	2.22	0.57	54
KF13	0.02	0.02	3	91%	8.5	1.95	0.21	1139

Note. The Mg# and elemental ratios are measured by ICP-MS, with uncertainty of 5%–10%, and calculated by their atom ratios.

isotope compositions in two of the three nonmagnetic, sulfide-rich fractions to lighter values in the nonmagnetic, silicate-rich, and Fe–Ni metal-rich, magnetic fractions (Table 2 and Figure 2). This is especially pronounced in the chondrites Indarch (EH4) and Khairpur (EL6) that experienced higher degrees of metamorphism. Also, the δ^{53}Cr values for nonmagnetic silicates become progressively lighter with the increasing metamorphic degree (Figure 2). Note that we report both the measured and calculated (by mass balance: bulk = magnetic + nonmagnetic sulfides + nonmagnetic silicates) δ^{53}Cr compositions for the magnetic components in the ECs in Table 2. The reason for this is that the metals (with high Fe/Cr ratios) in the ECs may exhibit elevated cosmogenic effects (Qin et al. 2010), which would shift the Cr stable isotope data obtained by the DS method and these isotopic anomalies may not be adequately corrected for. As such, we consider the calculated δ^{53}Cr values of the magnetic fractions as more likely to be accurate determinations of the primitive Cr stable isotope compositions of these fractions. The two EC chondrules (KF3 and KF13) extracted from SAH 97096 that have high Mg# [Mg/(Mg+Fe)∗100%; atom ratios; >90%] show heavier δ^{53}Cr values (0.04 ± 0.03‰; 2SD, $N = 2$) than the bulk ECs, while one Fe–Ni-bearing chondrule (KF10, with low Mg#, Mg/Ni ratios and high Fe/Cr ratios; Table 3) has a δ^{53}Cr value of –0.04 ± 0.03‰ (Table 3).

4. Discussion

4.1. δ^{53}Cr Variability among Chondrite Groups: Physical Conditions in the Solar Nebula

The δ^{53}Cr data set in this study covers almost all chondrite groups, thereby providing a Cr stable isotope panorama for chondrites. These new data indicate that the mass-dependent Cr isotope compositions of the chondrite groups are not as homogeneous as previously thought based on a more limited data set (Bonnand et al. 2016; Schoenberg et al. 2016; Zhu et al. 2021b). However, unlike the intragroup variability of the mass-independent Cr isotopic compositions (the deviation of

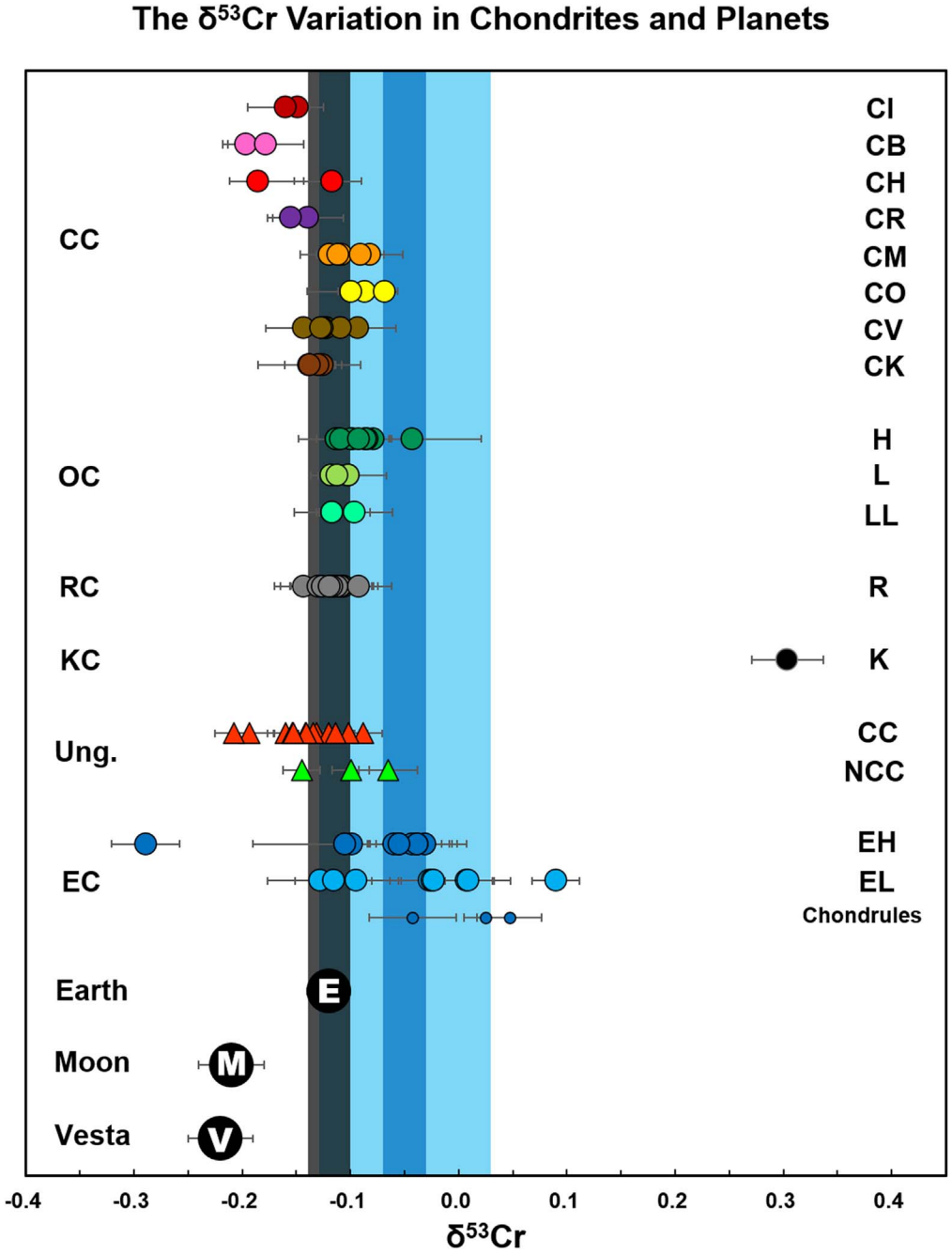

Figure 1. The Cr stable isotope variation of chondrites, chondrules, and terrestrial planets. The gray and blue shades represent the average δ^{53}Cr values, with uncertainty of 2SE for Earth and 2SD (light blue; –0.05 ± 0.08‰) and 2SE (dark blue; –0.05 ± 0.02‰) for ECs, NCC: non-carbonaceous chondrites, OC: ordinary chondrites, RC: Rumuruti chondrites, KC: Kakangari chondrites, Ung.: ungrouped chondrites, EC: enstatite chondrites. Chondrites from different groups have varied Cr stable isotope compositions (δ^{53}Cr values), suggesting different physical conditions of their accretion regions. The large δ^{53}Cr heterogeneity in ECs result from the mixing of sulfide phases that have high δ^{53}Cr values. The isotopically heavy Cr in EC chondrules are caused by Cr evaporation under reduced conditions. The δ^{53}Cr deficit between Earth and ECs likely reflect a volatile loss of Cr during molten planetesimal stages, which triggered equilibrium Cr stable isotope fractionation resulted in an isotopically heavier gas phase and a light residue.

the $^{54}Cr/^{52}Cr$ normalized ratios from a terrestrial standard, usually expressed as ε^{54}Cr values) (Trinquier et al. 2007; Qin et al. 2010; Zhu et al. 2021c), the mass-dependent δ^{53}Cr ranges within groups of carbonaceous, ordinary, and Rumuruti chondrites are quite homogeneous. For example, the CM, CO, and CV chondrites have the most variable ε^{54}Cr values (Zhu et al. 2021c), while their grouped δ^{53}Cr values are homogeneous: CM (δ^{53}Cr = –0.10 ± 0.03‰; 2SD, $N = 5$), CO (δ^{53}Cr = –0.08 ± 0.03‰; 2SD, $N = 3$) and CV (δ^{53}Cr = –0.12 ± 0.03‰; 2SD, $N = 8$). The exceptions are the ECs, which will be discussed in Section 4.2. Similar to these grouped chondrites, the δ^{53}Cr values of the ungrouped CCs and non-CCs overlap, while their mass-independent ε^{54}Cr values are distinct (Zhu et al. 2021a).

The chondrite δ^{53}Cr values are not correlated with the ε^{53}Cr (radiogenic) and ε^{54}Cr (nucleosynthetic) values (Trinquier et al. 2007; Qin et al. 2010; Zhu et al. 2021c), implying that the δ^{53}Cr variations among the chondrite groups are unlikely to originate from the same process that caused the mass-independent Cr isotope variability. Both Ca–Al-rich inclusions

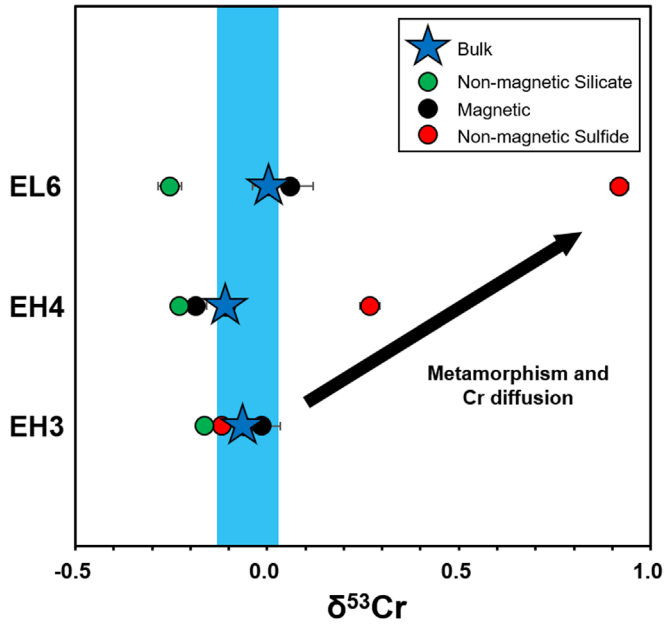

Figure 2. The Cr stable isotope compositions of different phases of ECs. The blue shaded area indicates the average δ^{53}Cr value of bulk ECs with 2SD uncertainty. The progressively heavy and light Cr in nonmagnetic sulfide and non-magmatic silicates, respectively, of petrological types from 3–6 suggests the Cr diffusion in the metamorphism processes.

(CAIs) and chondrules formed at high temperatures in the nebula that could potentially have fractionated Cr stable isotopes and, thus, their contributions to the bulk chondrites may cause Cr isotope variations in the bulk chondrites as observed for other elements (e.g., Pringle et al. 2017; Hu et al. 2021). Among the chondrite groups, CI chondrites contained few if any chondrules or CAIs, whereas the CV chondrites contain the most CAIs by volume and 45 vol% of chondrules (Krot et al. 2014), but the δ^{53}Cr values for bulk CI (–0.15 ± 0.01‰; 2SD) and CV (–0.12 ± 0.03‰; 2SD) chondrites are indistinguishable from each other. This observation, and the limited, overlapping δ^{53}Cr ranges between different CC groups suggest that variable relative proportions of chondrite components (i.e., chondrules, CAIs, and matrix) do not visibly affect the δ^{53}Cr variations among the bulk CCs. Chondrites from the same groups but with different degrees of aqueous alteration (e.g., CR1–CR2, CM1–CM2), thermal metamorphism (H3–H7 and R3–R6), or redox state ($CV3_{red}$, $CV3_{oxA}$ and $CV3_{oxB}$) also have comparable δ^{53}Cr values, suggesting that parent body processes did not alter the Cr stable isotope compositions at the scale of the samples analyzed here. As such, the δ^{53}Cr signatures of most bulk chondrites are likely primary, and record processes in the solar nebula, which is consistent with other metal isotope systems, e.g., Si (Armytage et al. 2011; Zambardi et al. 2013), Fe (Wang et al. 2014; Dauphas et al. 2017), Ni (Klaver et al. 2020; Wang et al. 2021), Ca (Valdes et al. 2014; Amsellem et al. 2017; Huang & Jacobsen 2017; Schiller et al. 2018) or Zn (Luck et al. 2005; Pringle et al. 2017). The subgroups of the OCs (H, L, and LL) also possess similar δ^{53}Cr values, indicating that nebular metal-silicate fractionation did not resolvable alter the Cr stable isotopic composition before chondrite accretion. However, for the EH and EL chondrites, because of the relatively large variations in δ^{53}Cr the situation is less clear. Assuming that in the ECs there are significant inter-mineral stable Cr isotope fractionations, mineralogical heterogeneity at the scale of our samples may explain the larger variations of δ^{53}Cr in our bulk analyses. This will be discussed further below.

The CH and CB chondrites are metal-rich chondrites that are depleted in moderately volatile lithophile elements, e.g., Na, K, or Zn (Weisberg et al. 2001). The depletion was likely caused by evaporation due to impact events following parent body accretion (Krot et al. 2005), which has fractionated, for instance, their Zn (Pringle et al. 2017), Mg (Olsen et al. 2013) and Fe–Ni isotopes (Weyrauch et al. 2021). However, their bulk Cr stable isotope compositions are similar to CR chondrites (δ^{53}Cr = –0.15 ± 0.02‰; 2SD, $N = 2$), which are considered to belong to the same clan as CB-CH chondrites (Krot et al. 2014). Lack of Cr isotope fractionation in CB-CH chondrites is consistent with the fact that they do not appear to be depleted in Cr relative to other chondrites (Weisberg et al. 2001; Yamashita et al. 2010), which suggests that no significant Cr loss via evaporation occurred during or after the impact that formed the CB-CH chondrites.

LEW 87232 (K3) that has the heaviest isotopic composition (δ^{53}Cr = 0.30 ± 0.03‰) of the analyzed chondrites (from ~–0.3‰ to ~0.1‰) has also the lowest Cr content (1150 ppm; Weisberg et al. 1996). Furthermore, LEW 87232 is also depleted in Cr compared to other K chondrites, e.g., Kakangari (K3) has a Cr content of ~3600 ppm. The low Cr content of LEW 87232, relative to that of Kakangari, has been interpreted to be the product of terrestrial weathering (Weisberg et al. 1996). However, the low Cr content of LEW 87232 is unlikely to be a weathering product because (1) it has a heavy Cr isotope composition, whereas terrestrial weathering should result in an enrichment in the light Cr isotope (Frei et al. 2014); and (2) for other groups of chondrites (e.g., Rumuruti, CC, OC, and EC) that experienced varying degrees of weathering, there is no difference in Cr content (Kallemeyn & Wasson 1981, 1986; Kallemeyn et al. 1989, 1996) and isotope compositions (Bonnand et al. 2016; Schoenberg et al. 2016; this study) between the falls and finds. There are large differences in Cr and other elemental contents, Se, Zn, K, V, Ca, Mn, and Eu, spanning from volatile to refractory elements, between LEW 87232 and other two K chondrites (Weisberg et al. 1996), and also different O isotope compositions (Δ^{17}O values of –1.22 ± 0.08‰ and –1.75 ± 0.08‰, respectively) between LEW 87232 and Kakangari (Weisberg et al. 1996). We speculate that either the two meteorites originated from two distinct parent bodies or the K chondrite parent body accreted heterogeneously (e.g., Zhu et al. 2021c). Matrix material accounts for 70 vol% of LEW 87232 (Weisberg et al. 1996). The low Cr content of the bulk LEW 87232 sample is controlled by the very low Cr content of its matrix (Barosch et al. 2020), so the matrix of LEW 87232 may have a different origin compared to matrix material in other chondrites.

4.2. δ^{53}Cr Compositions of ECs and Their Chondrules: Metamorphism and Volatile Processing

As mentioned earlier and unlike other groups of chondrites, the ECs show large bulk δ^{53}Cr variations that range from –0.29 ± 0.03‰ (MIL 07028, EH3) to 0.09 ± 0.02‰ (Pillistfer, EL6). In order to better understand the origin of the Cr isotope variations among the ECs, we measured the δ^{53}Cr values in leachates of different mineral fractions (magnetic, nonmagnetic sulfide-rich, and nonmagnetic silicate-rich) in three ECs: Qingzhen (EH3), Indarch (EH4), and Khairpur (EL6) (Table 2 and Figure 2). The different fractions of Indarch (EH4) and

Khairpur (EL6) exhibit variable δ^{53}Cr values, whereas the variations are less pronounced in the fractions from Qingzhen (EH3). In Indarch and Khairpur, the nonmagnetic sulfide-rich fractions are isotopically *heavy*, with δ^{53}Cr values of up to ~0.92‰, and the δ^{53}Cr values for nonmagnetic, sulfide-rich fractions increase with the metamorphic degrees (–0.12‰, 0.27‰, and 0.92‰ for petrologic types 3 [Qingzhen], 4 [Indarch], and 6 [Khairpur], respectively; Figure 2). By contrast, the silicate phases become isotopically lighter with increasing petrologic type (Figure 2), and their average δ^{53}Cr value is –0.21 ± 0.05‰, compared to the average δ^{53}Cr value for bulk ECs of –0.05 ± 0.02‰. Metamorphism can result in the redistribution of Cr between phases (mainly silicate and sulfide), with isotopically heavier Cr preferentially entering the sulfide, predicted by ab initio calculation (Moynier et al. 2011a). The minor internal Cr isotopic variations in the unequilibrated Qingzhen, unlike in the more metamorphosed Indarch and Khairpur, is a clear indication that the redistribution of Cr during thermal metamorphism is the cause of the internal isotopic heterogeneity in the ECs. In the recent study of δ^{53}Cr variability in enstatite achondrites, including aubrites, their isotopically heavy Cr was interpreted as evidence for sulfur-rich core formation. This is believed to result in the Fe–Ni–S core material being enriched in light Cr, whereas the silicate part of the body retains a heavy Cr isotope signature (Zhu et al. 2021d). In the ECs there is no evidence for melting and segregation of metal-sulfide melts. Hence, a more likely scenario for producing the bulk isotopic variability with sulfide fractions containing isotopically heavy Cr is Cr diffusion during metamorphism (kinetic isotope fractionation) and a heterogeneous distribution of sulfides at the scale of our samples.

Note that metamorphism should not modify the δ^{53}Cr values of the bulk meteorites unless the redistribution of Cr (and sulfides) occurred on scales that are larger than our bulk samples. The EC bulk δ^{53}Cr values are not correlated with their metamorphic grades. Hence, we may consider the δ^{53}Cr data for all the bulk EC samples with varied metamorphic degrees represent the Cr stable isotope composition of the EC reservoir. As mentioned before, the δ^{53}Cr heterogeneities between silicate-metal-sulfide phases in the ECs may cause the δ^{53}Cr variations among bulk ECs. For example, Pillistfer (EL6) with its extreme δ^{53}Cr value, possesses anomalous Cr, Fe, and Ni contents of 942 ppm, 528,076 ppm, 40,295 ppm, respectively, and Mg# of 32% (analyzed in this study), compared to the chemistry for most of other ELs, with Cr, Fe, and Ni contents of ~3000 ppm, ~200,000 ppm and ~120,000 ppm, respectively (Kallemeyn & Wasson 1986). The large chemical difference between Pillistfer and other ECs could be caused by its anomalous sample heterogeneity. However, the origin of the very low δ^{53}Cr value for MIL 07028 (EH3) that has a typical bulk EH composition is unknown. If we exclude these two samples (Pillistfer and MIL 07028) with extreme values, the rest of the 17 ECs possessed δ^{53}Cr values ranging from –0.13‰ to 0.01‰, with an average value of –0.05 ± 0.08‰ (2SD) or ± 0.02‰ (2SE).

The δ^{53}Cr data for EC chondrules are reported in Table 3 and Figure 1. Two of the three chondrules (KF3 and KF13) have δ^{53}Cr values that are higher than the bulk of their host chondrite SAH 97096 (EH3), whereas the δ^{53}Cr value of KF10 is slightly lighter than the bulk. While we could not analyze the absolute Cr content of these chondrules (their small size prevented a precise measurement of their bulk weight), we can compare their volatile depletion based on the ratio of a moderately volatile element over a refractory element, i.e., Na/Al (both Na and Al are not siderophile). The similar Na/Al ratios among the three chondrules indicate that they should have a similar volatile-element content, and that therefore the δ^{53}Cr differences between the three chondrules is unlikely to be controlled by volatile loss. Note that KF10 has a higher Fe and Ni content (i.e., low Mg# and Mg/Ni ratios) than KF3 and KF13 and most of the other EH chondrules for which we have data (Zhu et al. 2020b). The low Mg/Ni ratio of chondrule KF10 indicates the presence of some metal and/or sulfide grains (typical EC chondrules are dominated by only enstatite) that has a lighter isotopic Cr composition. Hence, the δ^{53}Cr value of KF10 likely includes metal and sulfide (including troilite) and would not be representative of the silicate fraction of the chondrule. In contrast to the metal/sulfide-bearing KF10, the heavy Cr isotope signatures of KF3 and KF13, relative to their host chondrite SAH 97096, may reflect Cr isotope fractionation during melting and evaporation, where the high-temperature silicate–SiO reaction takes place (Tanaka & Nakamura 2017). Since the EC chondrule-forming disk region was highly reduced (fO_2 relative to the Iron- wüstite buffer (IW) of –8 to –10 log units (Righter et al. 2006; Grossman et al. 2008), Cr would not be oxidized in the gas phases during chondrule formation. As a result, both kinetic (the residues get enriched in heavy Cr) and equilibrium (the more oxidized species get enriched in heavy Cr) Cr isotope fractionation may have induced enrichment of isotopically heavy Cr in the chondrule silicates, which is consistent with our data. Similarly, EC chondrules also possess broadly heavier Si isotopes than bulk ECs, which has been interpreted as reflecting partial volatile loss of Si and recondensation of lighter Si into matrix silicates (Kadlag et al. 2019). This volatility-controlled stable isotope fractionation of EC chondrules, which caused Mn/Cr fractionation among EC components, occurred at 4565.7 ± 0.7 Ma as indicated by ^{53}Mn–^{53}Cr chronometry (Zhu et al. 2020b).

4.3. δ^{53}Cr Difference between Earth and ECs: Planetary Degassing?

The mean δ^{53}Cr value of bulk ECs (excluding Pillistfer and MIL 07028) is systematically higher (–0.05 ± 0.02‰, 2SE; ± 0.08‰, 2SD; $N = 17$) than that of the bulk silicate Earth (BSE) (–0.12 ± 0.02‰, 2SE), estimated from selected mantle peridotites and komatiites (Sossi et al. 2018; Jerram et al. 2020). We tested the significance of the δ^{53}Cr isotopic difference between the ECs and Earth by running an unpaired student's t-test using *Prism 8* (An unpaired t test compares the means of two independent or unrelated groups. In an unpaired t-test, the variance between groups is assumed to be equal), which returned a P-value of 0.002 confirming the statistical difference between the ECs and Earth (statistical difference is considered for the P-value < 0.05). ECs and Earth have indistinguishable mass-independent isotopic compositions for multiple elements, including Cr (Trinquier et al. 2007; Javoy et al. 2010; Qin et al. 2010; Mougel et al. 2018; Zhu et al. 2020b). Here, we assume that the initial Cr isotopic composition of the bulk Earth (BE) was also indistinguishable from that of ECs, which implies that the difference in δ^{53}Cr of 0.07 ± 0.03‰ between the ECs and Earth (Figure 1) was caused by planetary processes during Earth accretion and evolution.

Chromium is a siderophile element, especially under reduced conditions and high temperatures (Wood et al. 2008), and it is

believed that ~60% of the BE Cr was sequestered into the core during terrestrial core–mantle differentiation (Allègre et al. 1995; McDonough & Sun 1995). However, because of the high temperatures of terrestrial core formation conditions, Cr stable isotope fractionation between metal and silicate phases must have been small or even negligible (Moynier et al. 2011b; Bonnand et al. 2016). Furthermore, core formation is also predicted to preferentially enrich the metal in the lighter isotopes, leaving an isotopically heavy mantle (Moynier et al. 2011b). This is contrary to what is observed here between the ECs and the BSE. Therefore, terrestrial core formation is unlikely to be the cause of the presumed Cr stable isotope offset between the ECs and the BSE.

Because Cr can be isotopically fractionated by evaporation/condensation (Sossi et al. 2018; Zhu et al. 2019b), the potential Cr stable isotope difference between the BSE and the ECs might have been caused by volatilization of Cr in the same way that other elements seem to have been fractionated during the formation of Earth (e.g., Pringle et al. 2014; Hin et al. 2017; Norris & Wood 2017; Young et al. 2019). In detail, a light Cr isotope enrichment in Earth compared to the ECs would be consistent with equilibrium Cr isotope fractionation, which mimics Cr depletion during Moon and Vesta differentiation (e.g., Sossi et al. 2018; Zhu et al. 2019b).

This Cr depletion cannot have taken place during a terrestrial magma ocean event, e.g., following the Moon-formation giant impact (Wiechert et al. 2001) because gravity prevents heavy elements such as Cr from escaping from Earth, and may have actually had the inverse effect of replenishing Earth with impactor volatiles (Charnoz & Michaut 2015; Hin et al. 2017; Charnoz et al. 2021). On the other hand, Earth may have acquired its relatively heavy Cr isotope composition by vapor-melt fractionation from its precursor planetesimals. Intensive impacts and the decay of ^{26}Al (with a half-life of 0.7 million yr) would have heated and melted planetesimals, and thus, effective H loss that would increase the fO_2 (Schaefer & Fegley 2017) and make the evaporated Cr exist as multiple oxidized species in vapor as suggested for Vesta and the Moon (Sossi et al. 2018; Zhu et al. 2019b). In fact, this volatile depletion should occur in the first 3 million yr after solar system formation, as estimated from the lower ^{55}Mn/^{52}Cr and radiogenic ^{53}Cr/^{52}Cr (i.e., ε^{53}Cr) ratios in Earth compared to the ECs (Zhu et al. 2021c), which is consistent with the ages of planetesimals, i.e., 0–4 Ma after solar system formation (Amelin & Ireland 2013). Such equilibrium Cr stable isotope fractionation between the vapor and melt of planetesimals would also be consistent with the ~0.02‰ higher ^{25}Mg/^{24}Mg ratio of Earth compared to the ECs (Hin et al. 2017). The EC-Earth isotope difference also works for Si ($Tc_{50\%} = 1310$ K) with a δ^{30}Si difference of ~0.4‰ (Fitoussi & Bourdon 2012; Savage & Moynier 2013; Moynier et al. 2020), which because of high core formation temperatures in Earth, likely was not caused by core formation but by equilibrium Si isotope fractionation during evaporation or condensation (Pringle et al. 2014; Kadlag et al. 2019; Young et al. 2019). Note that OCs and some CCs also have Mg and Si isotopes that are lighter than the BSE (Armytage et al. 2011; Savage & Moynier 2013; Hin et al. 2017; Moynier et al. 2020), but for Cr, only the ECs show a small resolvable δ^{53}Cr difference from the BSE, while CCs and OCs share a common δ^{53}Cr composition with BSE.

Based on various compositional arguments (e.g., Palme & O'Neill 2014) and the radiogenic ε^{53}Cr the difference between the BSE and ECs (Trinquier et al. 2007; Qin et al. 2010; Mougel et al. 2018), Earth cannot originate directly from melting of ECs (Zhu et al. 2021c). Thus, other possible scenarios accounting for the δ^{53}Cr difference between the BSE and ECs deserve to be discussed. For instance, the δ^{53}Cr difference between the BSE and ECs can be related to the processes that also changed their bulk compositional difference (e.g., Mg/Si ratio). Previous studies proposed that in the feeding zone of the accreting Earth materials possessed the same mass-independent Cr isotope compositions, but some of Earth's precursor bodies and the ECs may have condensed in different sequences and ceased equilibrating with the gas at different temperatures, i.e., Earth at ~1400 K and ECs at <1250 K (Grossman et al. 2008; Morbidelli et al. 2020). Because of their different nebular histories (e.g., condensation) Earth and EC materials may have differed in their elemental and perhaps also stable isotope signatures, e.g., Si (Dauphas et al. 2015; Kadlag et al.2019). For example, in the primitive Qingzhen (EH3), the magnetic fractions (~–0.02‰) have higher δ^{53}Cr values than nonmagnetic sulfide and silicate-rich fractions (–0.16‰ to –0.12‰) (Table 2). Alternatively, precursor bodies of Earth and ECs may have undergone different volatilization processes, which may have resulted in their different δ^{53}Cr compositions (Miyazaki & Korenaga 2021). Thus, differential evaporation of Earth and EC precursors is also a possible way to shape their chemical and isotope features.

5. Conclusions

This study reports the mass-dependent Cr isotope composition of numerous chondrite types (including a comprehensive suite of ECs), leaching of ECs as well as chondrules from a primitive EH chondrite, using both MC-ICP-MS and TIMS. We observed a Cr stable isotope heterogeneity in chondrites, and their δ^{53}Cr values ranges from –0.29 ± 0.03‰ for (MIL 07028, EH3) to +0.30 ± 0.03‰ for (LEW 87232, K3), which we interpret to reflect the different physical conditions at different accretion regions for the chondrite parent bodies.

ECs show large intragroup δ^{53}Cr heterogeneities that may result from mixing of different phases; parent body thermal metamorphism likely caused heavy Cr enrichment in the sulfide-like phases. The EH chondrules show isotopically heavy Cr compared to their bulk host chondrite, which is caused by Cr loss at reduced conditions during chondrule-forming events.

Earth possesses systematically lower δ^{53}Cr values than bulk ECs. This might be because ECs do not faithfully record their initial Cr isotope signature, suggested by the intragroup variance in Cr stable isotope compositions. Assuming that ECs are the precursor materials of Earth and their average Cr isotope signature is representative of this material, the isotope difference between them (δ^{53}Cr = 0.07 ± 0.03‰) may be caused by equilibrium isotope fraction of Cr evaporation from reduced residue and oxidized gas phases. The low-temperature Cr loss suggests that the volatile depletion occurred at the terrestrial magma ocean stages or it may reflect the difference of condensation temperature between Earth and the EC parent body.

We thank Faith Vilas for editorial handling and two anonymous reviewers for constructive comments that greatly improve the quality of the paper. K.Z. thanks the Alexander von Humboldt Foundation for a postdoctoral fellowship, the

China Scholarship Council (CSC) for a PhD fellowship (#201706340161), and guest fellowships from CRC-TRR 170 (host: Harry Becker) and Purple Mountain Observation, CAS (host: Weibiao Hsu and Yun Jiang) for during his stay in Berlin (fall 2020) and Nanjing (summer 2021), respectively. F.M. acknowledges funding from the European Research Council under the H2020 framework program/ERC Starting Grant Agreement (#637503-PRISTINE) and financial support of the UnivEarthS Labex program at Sorbonne Paris Cité (#ANR-10-LABX-0023 and #ANR-11-IDEX-0005-02), and the ANR through a chaire d'excellence Sorbonne Paris Cité. Parts of this work were supported by IPGP multidisciplinary program PARI, by Region île-de-France SESAME grants No. 12015908, EX047016 and the IdEx Université de Paris grant, ANR-18-IDEX-0001 and the DIM ACAV+. Pierre Burckel and Pascale Louvat were appreciated for analysis on ICP-MS and MC-ICP-MS at IPGP, respectively, and Monika Feth, Maren Saenz, and Elis Hoffmann for help on the TIMS at FUB. H.B. is funded by the Deutsche Forschungsgemeinschaft (DFG, German Research Foundation–#263649064-TRR 170). Arizona State University's Center for Meteorite Studies is thanked for providing some of the samples analyzed in this work. US Antarctic meteorite samples were recovered by the Antarctic Search for Meteorites (ANSMET) program, which has been funded by NSF and NASA, and characterized and curated by the Department of Mineral Sciences of the Smithsonian Institution and the Astromaterials Acquisition and Curation Office at NASA Johnson Space Center. This is TRR 170 publication no. 143.

Appendix

In appendix, we firstly compare the Cr stable isotope data for same samples (ordinary chondrites from same solution) via double spike (DS) and sample-standard bracketing (SSB) methods (A1). Then, we showed the Backscattered electron (BSE) images for the EC chondrules studied in the work (A2). Finally we compared the Cr stable isotope data produced by MC-ICP-MS and TIMS (A3). The detailed discussion can be found in the figure captions.

A.1. Comparison for Cr Stable Isotope Data by DS and SSB Techniques

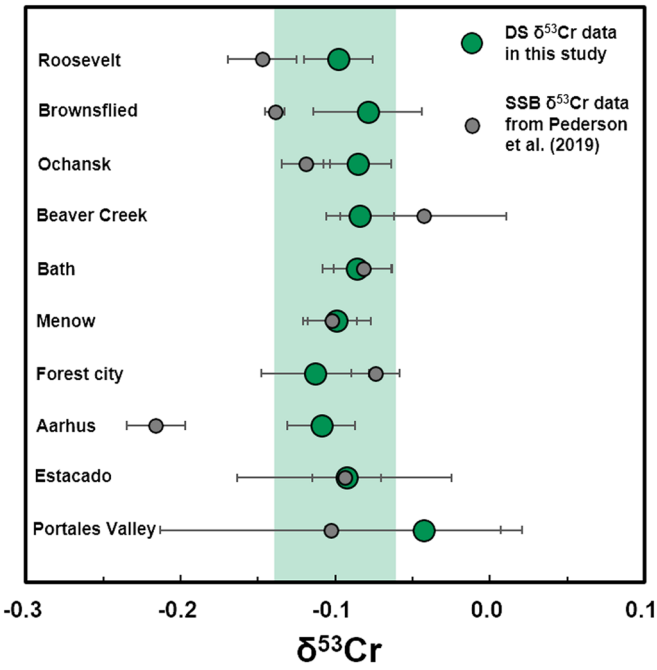

Figure A1. Comparison for Cr stable isotope data (with error of 2SD) by DS (large green circles) and SSB (small green circles) techniques. The green shaded area represents the δ^{53}Cr values for OCs (0.10 ± 0.04‰ 2SD, $N = 18$) Note that two data sets are from same sample dissolutions, and the yield of Cr purification for the SSB δ^{53}Cr data is 99% (Pedersen et al. 2019). Most of the data are consistent, while the largest discrepancy is ~0.1‰ (Aarhus). Therefore, we recommend that high-yield SSB method for Cr stable isotope measurements may be used to the low-temperature geochemistry of which Cr isotope fractionations can be up to several per miles (e.g., Konhauser et al. 2011), but not suitable to apply to high-temperature geochemistry, due to the limited Cr isotope fractionation.

Table A1
The δ^{53}Cr Data of H Chondrites from Same Dissolution Measured by the DS and SB (Data are from Pedersen et al. 2019) Techniques, Respectively

Sample	Type	δ^{53}Cr-DS	2SD	2SE	*N*	δ^{53}Cr-SSB	2SD	2SE	*N*
Roosevelt	H3.4	–0.098	0.022	0.016	2	–0.147	0.022	0.007	10
Brownfield 1937	H3.7	–0.079	0.035	0.020	3	–0.139	0.006	0.002	10
Ochansk	H4	–0.086	0.022	0.016	2	–0.119	0.016	0.005	10
Beaver Creek	H4	–0.084	0.022	0.016	2	–0.043	0.054	0.017	10
Bath	H4	–0.086	0.022	0.016	2	–0.082	0.019	0.006	10
Menow	H4	–0.099	0.022	0.016	2	–0.102	0.016	0.005	10
Forest City	H5	–0.113	0.035	0.020	3	–0.074	0.016	0.005	10
Aarhus	H6	–0.109	0.022	0.016	2	–0.216	0.019	0.006	10
Estacado	H6	–0.093	0.022	0.016	2	–0.094	0.070	0.022	10
Portales Valley	H6/7	–0.043	0.064	0.045	2	–0.103	0.110	Replicates	20

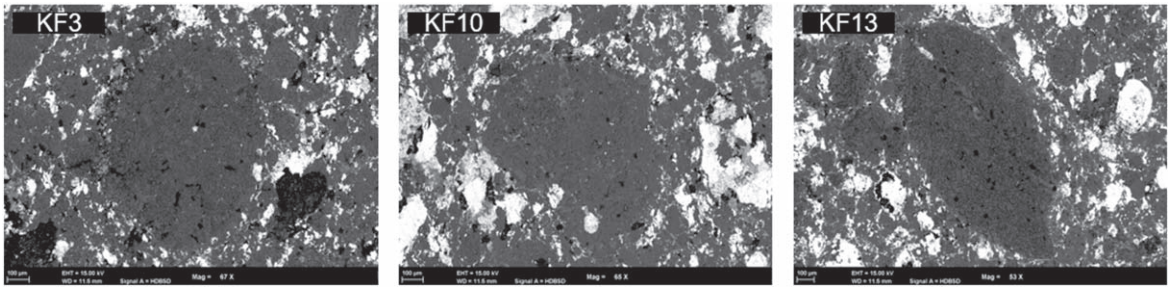

Figure A2. BSE images of the three EC chondrules.

A.2. BSE Images of the EC Chondrules

A.3. Comparison of Cr Stable Isotope Measurements by MC-ICP-MS and TIMS

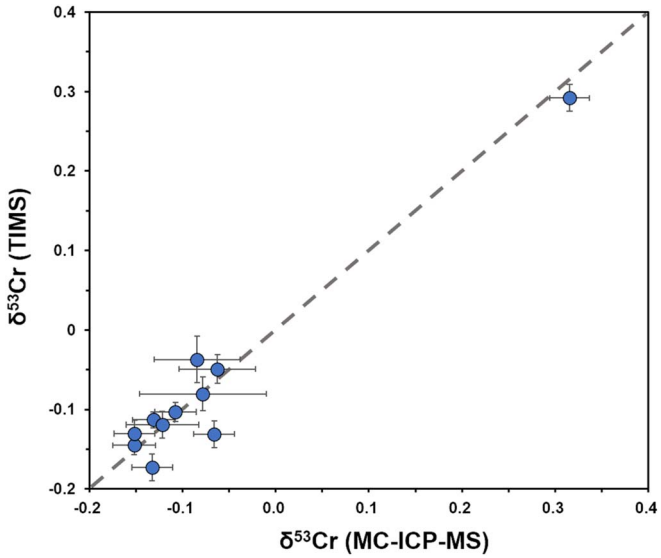

Figure A3. Comparison of Cr stable isotope measurements by MC-ICP-MS and TIMS. Note that the δ^{53}Cr data for same samples measured by MC-ICP-MS and TIMS are plotted in the *X*-axis and *Y*-axis, respectively. The replicated data are used their average values with 2SD uncertainty. The gray dashed line is the "1:1" relationship. Most of the δ^{53}Cr data are consistent, while some inconsistent data (e.g., SAH 97096) might be caused by sample heterogeneity.

ORCID iDs

Ke Zhu (朱柯) https://orcid.org/0000-0003-3613-7239
Conel M. O'D. Alexander https://orcid.org/0000-0002-8558-1427
Martin Schiller https://orcid.org/0000-0003-4149-0627
Martin Bizzarro https://orcid.org/0000-0001-9966-2124

References

Allègre, C., Manhès, G., & Lewin, É. 2001, E&PSL, 185, 49
Allègre, C. J., Poirier, J.-P., Humler, E., & Hofmann, A. W. 1995, E&PSL, 134, 515
Amelin, Y., & Ireland, T. R. 2013, Eleme, 9, 39
Amsellem, E., Moynier, F., Pringle, E. A., et al. 2017, E&PSL, 469, 75
Armytage, R. M. G., Georg, R. B., Savage, P. S., Williams, H. M., & Halliday, A. N. 2011, GeCoA, 75, 3662
Barosch, J., Ebel, D. S., Hezel, D. C., Alpert, S., & Palme, H. 2020, E&PSL, 542, 116286
Bloom, H., Lodders, K., Chen, H., et al. 2020, GeCoA, 277, 111
Bonnand, P., Williams, H. M., Parkinson, I. J., Wood, B. J., & Halliday, A. N. 2016, E&PSL, 435, 14
Braukmüller, N., Wombacher, F., Funk, C., & Münker, C. 2019, NatGe, 12, 564
Charnoz, S., & Michaut, C. 2015, Icar, 260, 440
Charnoz, S., Sossi, P. A., Lee, Y.-N., et al. 2021, Icar, 364, 114451
Chase, M. 1998, NIST–JANAF Thermochemical Tables (New York: AIP)
Connelly, J. N., Bizzarro, M., Krot, A. N., et al. 2012, Sci, 338, 651
Dauphas, N., John, S. G., & Rouxel, O. 2017, RvMG, 82, 415
Dauphas, N., Poitrasson, F., Burkhardt, C., Kobayashi, H., & Kurosawa, K. 2015, E&PSL, 427, 236
Fitoussi, C., & Bourdon, B. 2012, Sci, 335, 1477
Frei, R., Poiré, D., & Frei, K. M. 2014, ChGeo, 381, 110
Grossman, L., Beckett, J. R., Fedkin, A. V., Simon, S. B., & Ciesla, F. J. 2008, RvMG, 68, 93
Halliday, A. N., & Porcelli, D. 2001, E&PSL, 192, 545
Hellmann, J. L., Hopp, T., Burkhardt, C., et al. 2021, GeCoA, 309, 313
Hewins, R. H. 1997, AREPS, 25, 61
Hin, R. C., Coath, C. D., Carter, P. J., et al. 2017, Natur, 549, 511
Hu, J. Y., Dauphas, N., Tissot, F. L. H., et al. 2021, SciA, 7, eabc2962
Huang, S., & Jacobsen, S. B. 2017, GeCoA, 201, 364
Humayun, M., & Clayton, R. N. 1995, GeCoA, 59, 2131
Inglis, E. C., Creech, J. B., Deng, Z., & Moynier, F. 2018, ChGeo, 493, 544
Javoy, M., Kaminski, E., Guyot, F., et al. 2010, E&PSL, 293, 259
Jerram, M., Bonnand, P., Kerr, A. C., et al. 2020, ChGeo, 551, 119761
Johansen, A., Low, M.-M. M., Lacerda, P., & Bizzarro, M. 2015, SciA, 1, e1500109
Johansen, A., Ronnet, T., Bizzarro, M., et al. 2021, SciA, 7, eabc0444
Kadlag, Y., Tatzel, M., Frick, D. A., & Becker, H. 2019, GeCoA, 267, 300
Kallemeyn, G. W., Rubin, A. E., Wang, D., & Wasson, J. T. 1989, GeCoA, 53, 2747
Kallemeyn, G. W., Rubin, A. E., & Wasson, J. T. 1996, GeCoA, 60, 2243
Kallemeyn, G. W., & Wasson, J. T. 1981, GeCoA, 45, 1217
Kallemeyn, G. W., & Wasson, J. T. 1986, GeCoA, 50, 2153
Kato, C., & Moynier, F. 2017a, SciA, 3, e1700571
Kato, C., & Moynier, F. 2017b, E&PSL, 479, 330
Klaver, M., Ionov, D. A., Takazawa, E., & Elliott, T. 2020, GeCoA, 268, 405
Konhauser, K. O., Lalonde, S. V., Planavsky, N. J., et al. 2011, Natur, 478, 369
Krot, A. N., Amelin, Y., Cassen, P., & Meibom, A. 2005, Natur, 436, 989
Krot, A. N., Keil, K., Scott, E. R. D., Goodrich, C. A., & Weisberg, M. K. 2014, in Treatise on Geochemistry, ed. H. D. Holland & K. K. Turekian (2nd ed.; Oxford: Elsevier), 1
Lodders, K. 2003, ApJ, 591, 1220
Luck, J.-M., Othman, D. B., & Albarède, F. 2005, GeCoA, 69, 5351
Mahan, B., Moynier, F., Siebert, J., et al. 2018, PNAS, 115, 8547
McDonough, W. F., & Sun, S.-S. 1995, ChGeo, 120, 223
Miyazaki, Y., & Korenaga, J. 2021, Icar, 361, 114368
Morbidelli, A., Libourel, G., Palme, H., Jacobson, S. A., & Rubie, D. C. 2020, E&PSL, 538, 116220

Mougel, B., Moynier, F., & Göpel, C. 2018, E&PSL, 481, 1
Moynier, F., Deng, Z., Lanteri, A., et al. 2020, E&PSL, 549, 116468
Moynier, F., & Fegley, B., Jr. 2015, in The Early Earth: Accretion and Differentiation, ed. J. Badro & M. Walter, Vol. 212 (New York: Wiley), 27
Moynier, F., Paniello, R. C., Gounelle, M., et al. 2011a, GeCoA, 75, 297
Moynier, F., Yin, Q.-Z., & Schauble, E. 2011b, Sci, 331, 1417
Norris, C. A., & Wood, B. J. 2017, Natur, 549, 507
O'Neill, H. S. C., & Palme, H. 2008, RSPTA, 366, 4205
Olsen, M. B., Schiller, M., Krot, A. N., & Bizzarro, M. 2013, ApJL, 776, L1
Palme, H., & O'Neill, H. S. C. 2014, in Treatise on Geochemistry, ed. H. D. Holland & K. K. Turekian (2nd; Oxford: Elsevier), 1
Paniello, R. C., Day, J. M., & Moynier, F. 2012, Natur, 490, 376
Pedersen, S. G., Schiller, M., Connelly, J. N., & Bizzarro, M. 2019, M&PS, 54, 1215
Petitat, M., Birck, J.-L., Luu, T., & Gounelle, M. 2011, ApJ, 736, 23
Pringle, E. A., & Moynier, F. 2017, E&PSL, 473, 62
Pringle, E. A., Moynier, F., Beck, P., Paniello, R., & Hezel, D. C. 2017, E&PSL, 468, 62
Pringle, E. A., Moynier, F., Savage, P. S., Badro, J., & Barrat, J.-A. 2014, PNAS, 111, 17029
Qin, L., Alexander, C. M. O. D., Carlson, R. W., Horan, M. F., & Yokoyama, T. 2010, GeCoA, 74, 1122
Righter, K., Drake, M. J., & Scott, E. 2006, in Meteorites and the Early Solar System II, ed. D Lauretta, & H. Y. McSween, Jr (Tucson, AZ: Univ. of Arizona Press) 803
Savage, P. S., & Moynier, F. 2013, E&PSL, 361, 487
Schaefer, L., & Fegley, B., Jr. 2017, ApJ, 843, 120
Schiller, M., Bizzarro, M., & Fernandes, V. A. 2018, Natur, 555, 507
Schiller, M., Van Kooten, E., Holst, J. C., Olsen, M. B., & Bizzarro, M. 2014, J. Anal. At. Spectrom., 29, 1406
Schiller, M., Paton, C., & Bizzarro, M. 2015, GeCoA, 149, 88
Schoenberg, R., Merdian, A., Holmden, C., et al. 2016, GeCoA, 183, 14
Schoenberg, R., Zink, S., Staubwasser, M., & Von Blanckenburg, F. 2008, ChGeo, 249, 294
Schrader, D. L., Nagashima, K., Krot, A. N., et al. 2017, GeCoA, 201, 275
Scott, E. R. D., & Krot, A. N. 2014, in Treatise on Geochemistry, ed. H. D. Holland & K. K. Turekian (2nd ed.; Oxford: Elsevier), 65
Sossi, P., Moynier, F., & van Zuilen, K. 2018, PNAS, 115, 10920
Stracke, A., Palme, H., Gellissen, M., et al. 2012, GeCoA, 85, 114
Tanaka, R., & Nakamura, E. 2017, NatAs, 1, 0137
Torrano, Z. A., Schrader, D. L., Davidson, J., et al. 2021, GeCoA, 301, 70
Trinquier, A., Birck, J.-L., & Allègre, C. J. 2007, ApJ, 655, 1179
Trinquier, A., Birck, J.-L., & Allègre, C. J. 2008a, JAAS, 23, 1565
Trinquier, A., Birck, J. L., Allègre, C. J., Göpel, C., & Ulfbeck, D. 2008b, GeCoA, 72, 5146
Valdes, M. C., Moreira, M., Foriel, J., & Moynier, F. 2014, E&PSL, 394, 135
Visscher, C., & Fegley, B. 2013, ApJ, 767, L12
Wang, K., & Jacobsen, S. B. 2016, Natur, 538, 487
Wang, K., Savage, P. S., & Moynier, F. 2014, GeCoA, 142, 149
Wang, S.-J., Wang, W., Zhu, J.-M., et al. 2021, NatCo, 12, 294
Weisberg, M. K., Prinz, M., Clayton, R. N., et al. 1996, GeCoA, 60, 4253
Weisberg, M. K., Prinz, M., Clayton, R. N., et al. 2001, M&PS, 36, 401
Weyrauch, M., Zipfel, J., & Weyer, S. 2021, GeCoA, 308, 291
Wiechert, U., Halliday, A., Lee, D.-C., et al. 2001, Sci, 294, 345
Wood, B. J., Smythe, D. J., & Harrison, T. 2019, AmMin, 104, 844
Wood, B. J., Wade, J., & Kilburn, M. R. 2008, GeCoA, 72, 1415
Wu, G., Zhu, J.-M., Wang, X., Johnson, T. M., & Han, G. 2020, AnaCh, 92, 1463
Yamashita, K., Maruyama, S., Yamakawa, A., & Nakamura, E. 2010, ApJ, 723, 20
Yoshizaki, T., & McDonough, W. F. 2021, Geoch., 81, 125746
Young, E. D., Shahar, A., Nimmo, F., et al. 2019, Icar, 323, 1
Zambardi, T., Poitrasson, F., Corgne, A., et al. 2013, GeCoA, 121, 67
Zhu, J.-M., Wu, G., Wang, X., Han, G., & Zhang, L. 2018, JAAS, 33, 809
Zhu, K., Liu, J., Moynier, F., et al. 2019a, ApJ, 873, 82
Zhu, K., Moynier, F., Schiller, M., et al. 2020a, ApJ, 888, 126
Zhu, K., Moynier, F., Schiller, M., et al. 2021a, in 52nd Lunar and Planetary Science Conf. LPI Contribution (Houston, TX: Lunar and Planetary Institute), 2131
Zhu, K., Moynier, F., Schiller, M., et al. 2021b, GeCoA, 293, 598
Zhu, K., Moynier, F., Schiller, M., et al. 2021c, GeCoA, 301, 158
Zhu, K., Moynier, F., Schiller, M., et al. 2021d, GeCoA, 308, 256
Zhu, K., Moynier, F., Schiller, M., & Bizzarro, M. 2020b, ApJL, 894, L26
Zhu, K., Sossi, P. A., Siebert, J., & Moynier, F. 2019b, GeCoA, 266, 598